Chapter 4

Sliding Mode Speed and Position Control of Induction Motor Drive in Cascade Connection

Grzegorz Tarchała and Teresa Orłowska-Kowalska

Additional information is available at the end of the chapter

http://dx.doi.org/10.5772/63407

Abstract

This chapter deals with sliding mode application in control of an induction motor (IM) torque, speed, and position. Classical, direct approaches to control mentioned variables are described. Their drawbacks are presented and analyzed. Direct control structures are then compared with the proposed cascade sliding mode control structures. These structures allow to control all of the IM variables effectively, simultaneously ensuring supervision of all remaining variables. All of the analyzed structures are illustrated with block diagrams, as well as with simulation and experimental test results.

Keywords: induction motor, sliding mode control, torque control, speed control, position control

1. Introduction

Sliding mode control (SMC) is a commonly recognized robust control method. It is known to be independent on external disturbances [load torque in case of the induction motor (IM)] and internal changes (e.g., variation of motor parameters, due to heating). It can be successfully applied in control of all IM variables like flux, torque, speed and position [1]. However, it suffers from some characteristic negative features, such as steady-state and dynamical errors, chattering and variable switching frequency.

Over the several past decades, researchers tried to eliminate or reduce the disadvantages of the sliding mode applied to the IM control. The steady-state speed control error has been eliminated using the sliding surface with an additional integral part in reference [2]. Integral

part in the switching function has also been used to eliminate the dynamical and steady-state errors in the torque control [3].

Most of the papers focused on reducing the most negative feature of the SMC, i.e. chattering (large oscillations of controlled variables). Position control with adaptive continuous approximation of the sign function is proposed in reference [4]. Load torque estimator was introduced in reference [5] to reduce level of the discontinuous part of the control signal. One of the effective solutions to reduce the chattering is the application of higher-order sliding modes. They were introduced for all of the IM variables: torque in reference [6], speed (in a speed-sensorless approach) in reference [7] and position in reference [8]. The IM drive control, supplied from a current source inverter with the second-order SMC is introduced in reference [9]. Integral SMC of stator current components is shown in references [10–12] to reduce the chattering.

One of the chattering sources is a discretization caused by digital implementations of the drives' control structures; therefore, the discrete SMC methods have been proposed. The IM position discrete control is proposed in references [13] and [14]. The discrete SMC of the IM speed is introduced in reference [15].

Another drawback of the SMC in a direct approach (when the control algorithm defines the transistors' control signals directly) is a variable switching frequency. In order to eliminate this phenomenon, a voltage modulator can be applied. The classical direct torque control (DTC), SMC and space vector modulation (SVM) were combined in references [16] and [17]. Similarly, the indirect field-oriented control (IFOC) method and SMC were combined in reference [18].

In the past years, there have also been the attempts to extend the robustness of the IM control over the reaching phase, not only the sliding phase. The proposed approaches can be divided into two groups. In the first one, the switching line (or a surface) is designed to include the starting point: for speed control in reference [2] and for the position control in reference [19]. The second group consists of the methods with time-varying switching lines. They have been applied mainly in the position control [20], but also for the speed control [21].

In this chapter, a comparative analysis of the SMC of all IM state variables is presented. Direct approaches that define the transistor control signals directly are described and illustrated with simulation and experimental results. The cascade connection of sliding mode controllers is proposed for speed and position regulation, presented in a unified manner. The equivalent signal-based control is used to lower the level of the chattering in regulated variables.

This chapter consists of nine numerated sections. The following section presents the mathematical model of IM. Next three sections show the control of IM variables: torque, speed and position, respectively. Sections related to the speed and position control are divided into two subsections that include the direct and the cascade control. After short conclusions section, there is an appendix with experimental setup description and tables with tested IM parameters and base values, necessary to obtain the normalized unit system.

http://dx.doi.org/10.5772/63407

2. Mathematical model of induction motor drive

SMC algorithms are strictly based on the mathematical model of the controlled object, which is the IM in this research. This model will be shown in this section—it is created with commonly known simplifying assumptions [22]. It is written with normalized [per unit (p.u.)] units, in an arbitrary frame, rotating with the angular velocity ω_k. Base values, required to the p.u. system transformation, are shown in the appendix.

Stator and rotor voltage equations:

$$\mathbf{u_s} = r_s \mathbf{i_s} + T_N \frac{\mathrm{d}}{\mathrm{d}t} \boldsymbol{\psi}_\mathbf{s} + j\omega_k \boldsymbol{\psi}_\mathbf{s}, \tag{1}$$

$$\mathbf{u_r} = r_r \mathbf{i_r} + T_N \frac{\mathrm{d}}{\mathrm{d}t} \boldsymbol{\psi}_\mathbf{r} + j\left(\omega_k - \omega_m\right) \boldsymbol{\psi}_\mathbf{r}, \tag{2}$$

where $\mathbf{u_s} = u_{s\alpha} + ju_{s\beta}$, $\mathbf{u_r} = u_{r\alpha} + ju_{r\beta}$ are stator and rotor voltage vectors, $\mathbf{i_s} = i_{s\alpha} + ji_{s\beta}$, $\mathbf{i_r} = i_{r\alpha} + ji_{r\beta}$ are stator and rotor current vectors, $\boldsymbol{\psi}_\mathbf{s}=\psi_{s\alpha}+j\psi_{s\beta}$, $\boldsymbol{\psi}_\mathbf{r}=\psi_{r\alpha}+j\psi_{r\beta}$ are stator and rotor flux vectors, r_s, r_r are stator and rotor winding resistances, $T_\mathrm{N} = 1/(2\pi f_{sN})$ is nominal time constant, appearing after the per unit system is introduced, f_{sN} is nominal frequency of the motor and ω_m is mechanical velocity.

Flux equations:

$$\boldsymbol{\psi}_\mathbf{s} = l_s \mathbf{i_s} + l_m \mathbf{i_r} \tag{3}$$

$$\boldsymbol{\psi}_\mathbf{r} = l_r \mathbf{i_r} + l_m \mathbf{i_s}, \tag{4}$$

where $l_s = l_m + l_{s\sigma}$, $l_r = l_m + l_{r\sigma}$ are stator and rotor winding inductances, l_m is magnetizing inductance and $l_{s\sigma}$, $l_{r\sigma}$ are stator and rotor leakage inductances.

Electromagnetic torque and the motion equation are as follows:

$$m_e = \mathrm{Im}\left(\boldsymbol{\psi}_\mathbf{s}^* \mathbf{i_s}\right) = \psi_{s\alpha} i_{s\beta} - \psi_{s\beta} i_{s\alpha}, \tag{5}$$

$$\frac{\mathrm{d}\omega_m}{\mathrm{d}t} = \frac{1}{T_M}\left(m_e - m_o\right), \tag{6}$$

where m_e is electromagnetic torque, m_o is load torque and T_M is mechanical time constant of the drive.

It is assumed that the IM is supplied by an ideal voltage source inverter (VSI), which can be described by the following matrix equation:

$$\mathbf{u_s} = \begin{bmatrix} u_{s\alpha} \\ u_{s\beta} \end{bmatrix} = \frac{u_{DC}}{3}\mathbf{Tk}, \quad \mathbf{T} = \begin{bmatrix} 1 & -1/2 & -1/2 \\ 0 & \sqrt{3}/2 & -\sqrt{3}/2 \end{bmatrix}, \tag{7}$$

where $\mathbf{k} = [k_A, k_B, k_C]^T$ is the control signals' vector of the VSI transistors and u_{DC} is the DC-bus voltage.

3. Sliding mode direct torque control

In order to create a cascade connection of sliding mode controllers (for example torque and speed controllers), it is necessary to design first the sliding mode DTC. This method of control utilizes the IM mathematical model and its equations, shown in the previous chapter.

The first step in the designing is to define the so-called switching functions. The classical approach is first taken into account [1]:

$$\mathbf{s} = \begin{bmatrix} s_1 & s_2 & s_3 \end{bmatrix}^T, \tag{8}$$

where the components of **s** vector allow to control the motor torque, stator flux amplitude and to ensure the three-phase balance of the system, respectively:

$$s_1 = \alpha_1 \left(m_e^{ref} - m_e \right), \tag{9}$$

$$s_2 = \alpha_2 \left((\psi_s^{ref})^2 - \psi_s^2 \right), \tag{10}$$

$$s_3 = \alpha_3 \int \left(k_A + k_B + k_C \right) \mathrm{d}t, \tag{11}$$

where α_1, α_2, α_3 are control parameters, that need to be chosen.

The goal of the sliding mode controller will be to force the switching functions from Eqs. (9) to (11) to zero, which means that the real values will follow the reference ones. This goal can be achieved using the classical sliding-mode control formula, expressed as:

http://dx.doi.org/10.5772/63407

$$\begin{aligned} \mathbf{k} &= -\text{sign}(\mathbf{s}^*)^{\text{T}}, \\ \mathbf{s}^* &= \mathbf{s}^{\text{T}}\mathbf{D}, \end{aligned} \tag{12}$$

where the **D** matrix comes from the division of the switching function derivative into:

$$\dot{\mathbf{s}} = \mathbf{f} + \mathbf{D}\mathbf{k} \tag{13}$$

and can be calculated as follows:

$$\mathbf{D} = \begin{bmatrix} & \mathbf{D}_1 & \\ \alpha_3 & \alpha_3 & \alpha_3 \end{bmatrix}, \tag{14}$$

$$\mathbf{D}_1 = \frac{1}{T_N}\begin{bmatrix} \alpha_1\left(-i_{s\beta} + \dfrac{1}{x_s\sigma}\psi_{s\beta}\right) & \alpha_1\left(i_{s\alpha} - \dfrac{1}{x_s\sigma}\psi_{s\alpha}\right) \\ -2\alpha_2\psi_{s\alpha} & -2\alpha_2\psi_{s\beta} \end{bmatrix}\mathbf{T}. \tag{15}$$

In order to check the usefulness of the proposed control algorithm and to verify the stability of the proposed control system, the Lyapunov function method is applied. A positive defined Lyapunov function is proposed as follows:

$$L = \frac{1}{2}\mathbf{s}^{\text{T}}\mathbf{s} = \frac{1}{2}\left(s_1^2 + s_s^2 + \ldots + s_n^2\right) > 0. \tag{16}$$

Its derivative can be calculated as:

$$\begin{aligned} \dot{L} &= \mathbf{s}^{\text{T}}\dot{\mathbf{s}} = \\ &= \mathbf{s}^{\text{T}}\left(\mathbf{f} - \mathbf{D}\,\text{sign}(\mathbf{s}^*)^{\text{T}}\right) = \\ &= \mathbf{s}^{\text{T}}\mathbf{f} - \mathbf{I}\left|\mathbf{s}^{\text{T}}\mathbf{D}\right|^{\text{T}}, \end{aligned} \tag{17}$$

where $|\mathbf{s}^*| = [\,|s_1^*| \quad |s_2^*| \quad |s_3^*|\,]$, $\mathbf{I} = [1 \quad 1 \quad 1]$.

The stability inequality [negative value of Eq. (17)] is defined as:

$$|\mathbf{f}| < |\mathbf{D}|\mathbf{I}^{\text{T}}. \tag{18}$$

If the control parameters α_1, α_2, α_3, included in the **D** matrix in Eq. (14) are high enough to fulfill the condition [Eq. (18)], the system is stable and the real values follow their reference values.

Full SM-DTC block diagram is shown in **Figure 1**. The control structure defines the control signals k_A, k_B, k_C directly, to control the switches of the VSI without any voltage modulator. The input values are the reference values of stator flux amplitude and electromagnetic torque. If the speed exceeds the nominal value, the amplitude of the flux must be weakened in order to ensure the constant power operation of the induction machine.

It is also necessary to provide the measurement of the DC-bus voltage [this value is present in the **T** matrix in Eq. (14)] and stator phase currents (transformed to the stationary α-β frame from two-phase currents, when the three-phase symmetry is assumed). The control structure also needs estimated values, such as stator flux vector components (or its magnitude and angle) and electromagnetic torque (the hat "∧" indicates the estimated value). They must be determined by a proper estimator—this problem will not be addressed in this chapter. If the estimator requires the stator voltage vector knowledge, its components can be transformed from measured signals or calculated using the Eq. (7), taking into account the inverter dead-time [23].

The block diagram, shown in **Figure 1**, also emphasizes the digital implementation of the SM-DTC, together with the measurement delays (τ_d for current and voltage measurement and $\tau_{d\omega}$ for speed measurement). Nowadays, the continuous algorithms are realized in a discrete form using the digital signal processors (DSPs). The influence of the digital implementation will be shown in the following part of the chapter.

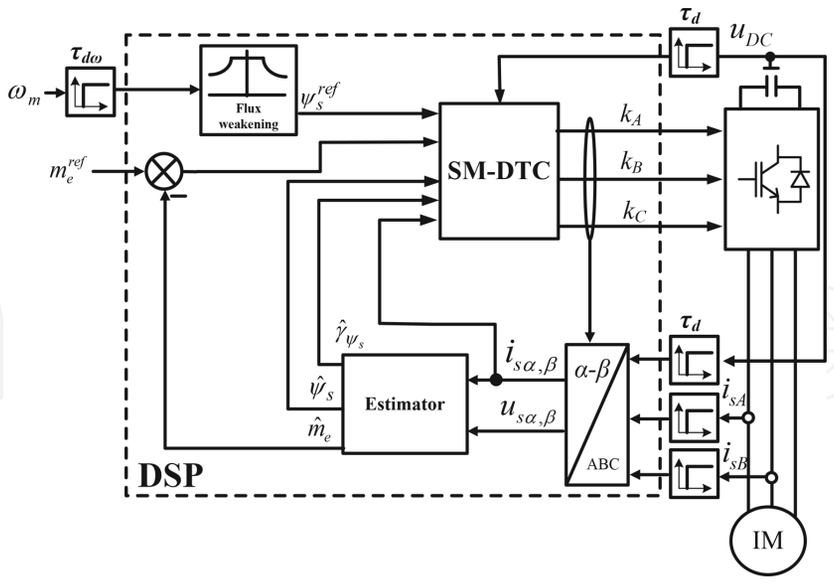

Figure 1. Block diagram of the SM-DTC (digital realization).

Figure 2 shows a comparative study of performance of the SM-DTC structure for three different cases: ideal simulation study (**Figure 2a**), simulation study with the DSP discretization taken into account (**Figure 2b**) and experimental results (**Figure 2c**).

http://dx.doi.org/10.5772/63407

Figure 2a shows the ideal operation of the SM-DTC and proves its perfect dynamical features. The torque and stator flux amplitudes follow their reference values almost immediately and without any oscillations. The speed is a result of the motor and load torque difference [according to Eq. (6)] and therefore is changing in a triangular way. Three-phase currents are smooth and sinusoidal—their frequency is changed automatically by the control structure.

Unfortunately, one of the negative properties of the SMC structures is the phenomenon called chattering [24]. There are many sources of the chattering—one of them is the discretization, connected with limited sampling rate of modern processors [25]. In order to check the influence of this phenomenon, special simulation model has been built. Suitable results are shown in **Figure 2b**. Large chattering (sometimes called the discretization chattering) can be seen in the controlled variables. It is also visible in phase currents. Due to the moment of inertia of the drive system, speed signal is still smooth.

Simulation test results have been validated using an experimental setup (see Appendix). Obtained results illustrate the same situation in a very similar way—the chattering can be seen in torque, flux and currents. The level of the obtained oscillations is even higher than during the simulation tests—it causes mechanical stress, dangerous for the drive, and acoustic noise.

One of the efficient solutions to avoid the chattering, visible in **Figure 2**, is to use the continuous approximation of the sign function. One of them is a saturation function:

$$\mathbf{d} = -0.5\left(\mathrm{sat}(\mathbf{s}^*, \varepsilon_{me})^{\mathrm{T}} + 1\right), \tag{19}$$

where ε_{me} is positive control parameter to be chosen and column vector $\mathbf{d} = [d_A, d_B, d_C]^{\mathrm{T}}$ is duty cycles' vector and the saturation function:

$$\mathrm{sat}(s) = \begin{cases} s/\varepsilon & \text{if } |s| \le \varepsilon \\ \mathrm{sign}(s) & \text{if } |s| > \varepsilon \end{cases}. \tag{20}$$

In this case, the control structure defines not the transistor control signals directly, but the duty cycle functions for each phase (relation of the switching-on time to the whole sampling period). Specific form of the Eq. (19) is imposed by the duty cycle feature—its values can vary between 0 and 1 (0% and 100%).

Effects of the saturation function usage are shown in **Figure 3a**. It can be seen that the oscillations level is greatly reduced. However, a significant and changing in time, regulation error can be seen in the electromagnetic torque transient. It can be eliminated using simple modification of the switching function [Eq. (9)], to obtain the following formula [3]:

$$s_1 = \alpha_1\left(m_e^{ref} - m_e\right) + K_I \int \left(m_e^{ref} - m_e\right) \mathrm{d}t \tag{21}$$

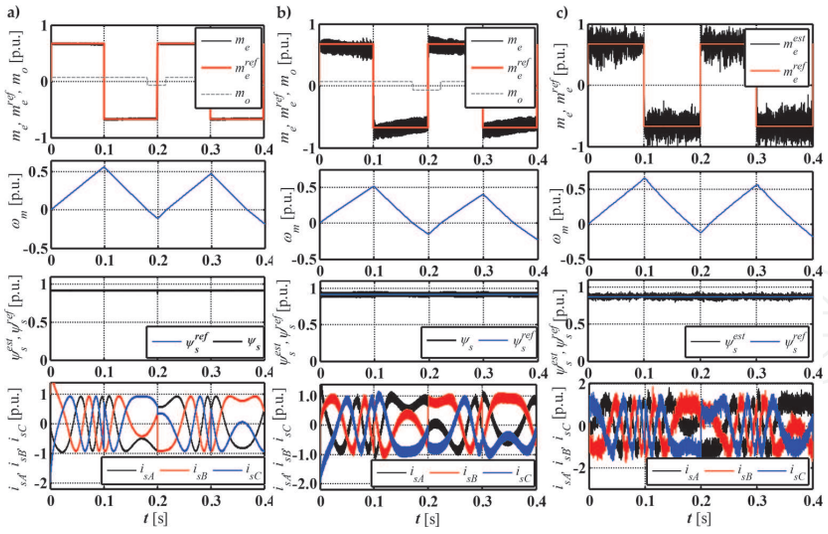

Figure 2. Performance of the SM-DTC for induction motor: (a) simulation study: ideal case, digital implementation is not taken into account, (b) simulation study: digital implementation taken into account, (c) experimental study; first row: reference and real (estimated) torque, second row: speed, third row: reference and real (estimated) stator flux, fourth row: phase currents.

where K_I is positive control parameter.

Results of the integral part introduction in the switching function are shown in **Figure 3b** and **3c** for simulation and experimental tests, respectively. The torque and stator flux are controlled perfectly, without any steady-state or dynamical errors. Additionally, the chattering phenomenon is reduced considerably—level of the oscillations in regulated signals is acceptable now.

Sliding mode DTC structure with the modified switching function, shown in this section, will be used to create the cascade speed and position control structures, shown in the following sections.

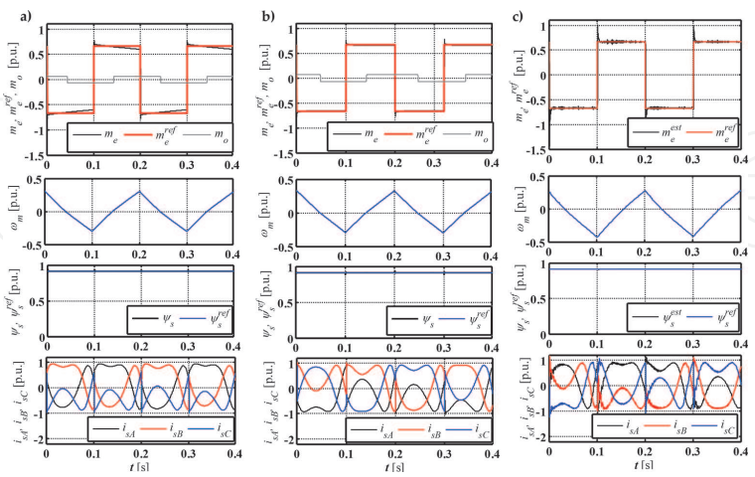

Figure 3. Performance of the SM-DTC for induction motor: (a) simulation study: saturation function used instead of the sign function, (b) simulation study: integral part added in the torque switching function, (c) experimental study; first row: reference and real (estimated) torque, second row: speed, third row: reference and real (estimated) stator flux, fourth row: phase currents.

http://dx.doi.org/10.5772/63407

4. Sliding mode speed control

4.1. Direct sliding mode speed control

The direct IM speed control can be realized very similarly to the DTC. The most significant difference is another switching function that can be expressed as in [1]:

$$s_1 = s_\omega = \alpha_1\left(\omega_m^{ref} - \omega_m - T_{c\omega}\dot{\omega}_m\right), \tag{22}$$

where $T_{c\omega}$ is time constant that defines the required dynamics of the speed.

When the switching function is zero, the controlled object acts as first-order inertia with time constant $T_{c\omega}$. Settling time of the system (95%) is equal to:

$$T_S = 3T_{c\omega}. \tag{23}$$

In this case, the same control algorithm [Eq. (12)] can be applied to regulate motor speed; however, the $\mathbf{D_1}$ matrix in Eq. (14) must be slightly modified (the additional term $T_{c\omega}/T_M$ appears):

$$\mathbf{D_1} = \frac{1}{T_N}\begin{bmatrix} \alpha_1\dfrac{T_{c\omega}}{T_M}\left(-i_{s\beta} + \dfrac{1}{x_s\sigma}\psi_{s\beta}\right) & \alpha_1\dfrac{T_{c\omega}}{T_M}\left(i_{s\alpha} - \dfrac{1}{x_s\sigma}\psi_{s\alpha}\right) \\ -2\alpha_2\psi_{s\alpha} & -2\alpha_2\psi_{s\beta} \end{bmatrix}\mathbf{T}. \tag{24}$$

The condition of the system stability remains the same as in Eq. (18).

The block diagram of the direct sliding mode speed control is shown in **Figure 4**. It is almost identical as the one shown in **Figure 1**; however, the speed switching function s_ω is provided instead of the torque regulation error. For the clarity of the block diagram, the digital realization and measurement delays will not be presented in the following figures.

Figure 5a shows the performance of the direct SM speed control structure in the ideal simulation case. The reverses of the speed are presented—the speed follows the reference value with the requested dynamics, which is indicated by the $\omega_m^{ref,dyn}$ signal. Even in this ideal case, the steady-state error exists—it is shown in the second row of **Figure 5a**. Additionally, electromagnetic torque of the motor is not controlled and supervised. Therefore, it exceeds the maximum value, set at the level 1.0 (it is about 150% of the nominal torque in p.u., see Appendix). If the digital realization of the control structure and measurement delays are taken into account, the steady-state speed error increases significantly—it can be seen in **Figure 5b**. Moreover, the torque and stator flux oscillation levels are much higher, similarly to the DTC

algorithm, shown in the previous section. If the saturation function is applied (**Figure 5c**), the regulation error becomes even larger; however, the chattering level is reduced. This simulation study is verified using the experimental tests (**Figure 5d**)—and both of them give almost the same results.

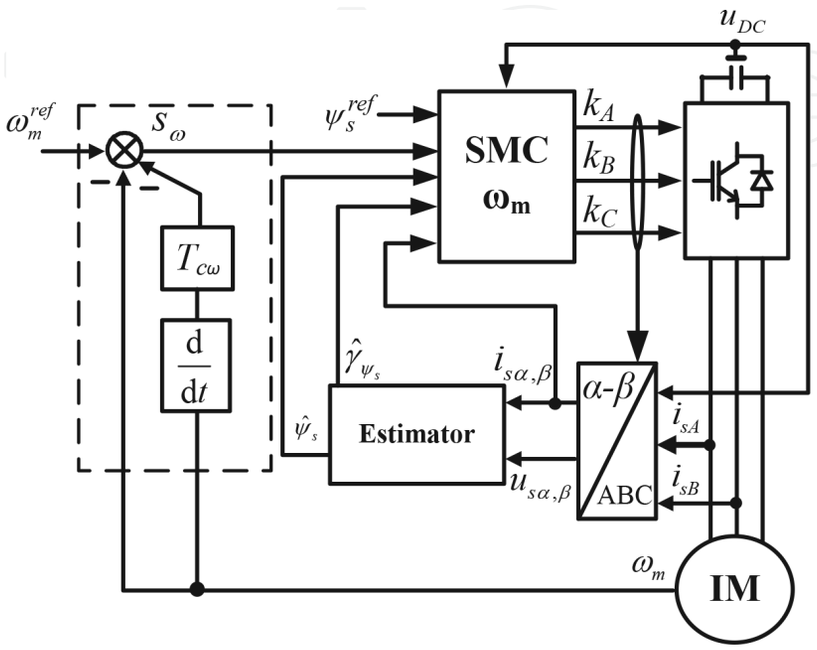

Figure 4. Block diagram of the direct SM speed control.

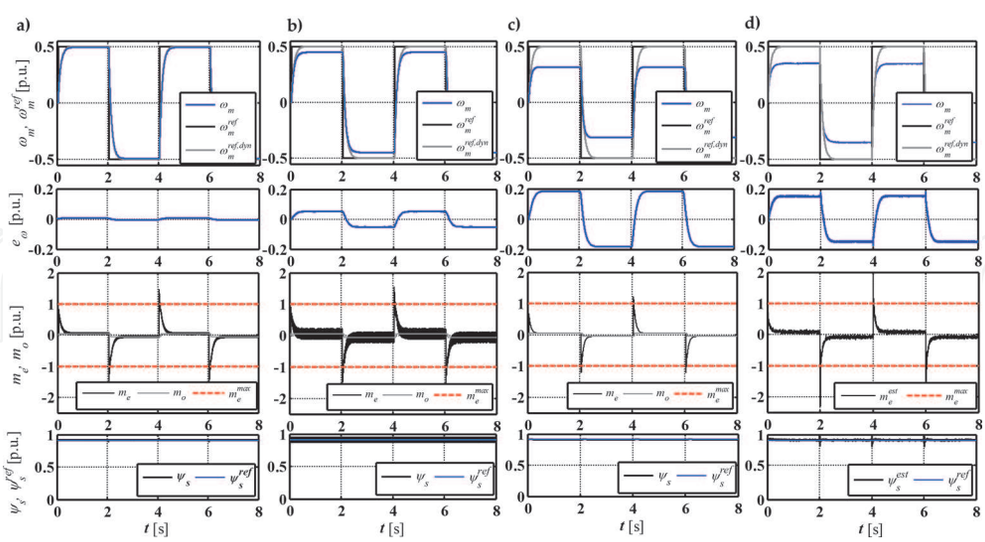

Figure 5. Performance of the SM direct speed control: (a) simulation study: control in the ideal case, (b) simulation study: speed control in case of the digital implementation and measurement delays taken into account, (c) simulation study: saturation function used instead of the sign function, (d) experimental tests results for saturation function usage; first row: reference and real speed, second row: speed control error, third row: load, electromagnetic and maximum torque, fourth row: reference and real amplitude of stator flux.

http://dx.doi.org/10.5772/63407

In both the previously mentioned cases, direct SM torque and speed control, the torque becomes higher than the acceptable level and can be dangerous for the drive and its mechanical elements. This drawback can be eliminated reducing the desired dynamics, defined by $T_{c\omega}$ or applying the cascade structure of the SM controllers. The second solution will be now described.

4.2. Cascade sliding mode speed control

In order to create the cascade connection of SM speed and torque regulators, the torque control loop has to be simplified to the first-order inertial element, described by the following transfer function:

$$\frac{m_e(p)}{m_e^{ref}(p)} = \frac{1}{T_{me}p+1}, \tag{25}$$

where p is Laplace operator, T_{me} is replacement time constant of the torque control circuit.

The control signals' vector becomes a scalar quantity $\mathbf{k}=[m_e^{ref}]$ and the switching functions' vector $\mathbf{s}=[s_\omega]$ likewise. In this case, the derivative of the switching function can be divided into:

$$\dot{s}_\omega = f_{1\omega} + f_{2\omega} + d_\omega m_e^{ref}, \tag{26}$$

where:

$$f_{1\omega} = \dot{\omega}_m^{ref} + \frac{T_{c\omega} - T_{me}}{T_M T_{me}} m_e, \tag{27}$$

$$f_{2\omega} = \frac{T_{c\omega}}{T_M}\dot{m}_o + \frac{1}{T_M} m_o, \tag{28}$$

$$d_\omega = -\frac{T_{c\omega}}{T_M T_{me}}. \tag{29}$$

In the above equations, $f_{1\omega}$ is the part that can be calculated from available variables, $f_{2\omega}$ depends on the unknown variables and d_ω stands next to the reference torque.

If the equivalent signal-based control method is applied, then the reference torque signal consists of two parts [26]:

$$m_e^{ref} = m_e^{ref,eq} + m_e^{ref,d}, \tag{30}$$

$$m_e^{ref,eq} = -\frac{1}{d_\omega} f_{1\omega}, \tag{31}$$

$$m_e^{ref,d} = -\frac{\Gamma_\omega^d}{d_\omega} \text{sign}(s_\omega), \tag{32}$$

where Γ_ω^d is a control parameter.

Continuous control signal part $m_e^{ref,eq}$ is calculated from available signals, and is designed to force the switching function to zero in presence of no load torque and motor parameters changes. The discontinuous part must be included in the SM control system, in order to compensate external disturbances, such as the load torque present in $f_{2\omega}$ and the inaccuracy of the simplification from Eq. (25). The switching function derivative becomes:

$$\dot{L} = s_\omega \dot{s}_\omega = s_\omega f_{2\omega} - \Gamma_\omega^d |s_\omega|, \tag{33}$$

while its negative value is ensured if:

$$\Gamma_\omega^d > |f_{2\omega}|. \tag{34}$$

Thus, if the control parameter is chosen properly, the stability of the proposed control system can be guaranteed. The block diagram of the cascade control structure described here is shown in **Figure 6**. Unlike the direct control from **Figure 4**, the speed controller output signal is the reference torque, and it consists of two parts. Furthermore, this signal can be limited at desired value. The reference torque is the input of the SM-DTC structure, described in the previous chapter.

Performance of the cascade SM speed control in presence of the passive load torque is shown in **Figure 7**. The obtained results are shown for the speed reverses. It can be seen that the speed follows the reference signal with required dynamics in all cases. First subfigure shows the relay control—the equivalent signal from Eq. (31) is not taken into account in this case and the control parameter is equal to $\Gamma_{me}^d = m_e^{max}$. Performance of the control structure is presented during simulation tests—despite the ideal conditions, some small dynamic and steady-state error appears. Due to the enormous mechanical vibrations, it is impossible to conduct the experimental tests. Therefore, the equivalent signal was taken into account and its performance is shown in **Figure 7b** and **7c** for simulation and experimental tests, respectively. The results are

http://dx.doi.org/10.5772/63407

almost the same. Electromagnetic torque has acceptable oscillations and is limited on a maximum value. Stator flux amplitude is kept constant at nominal value.

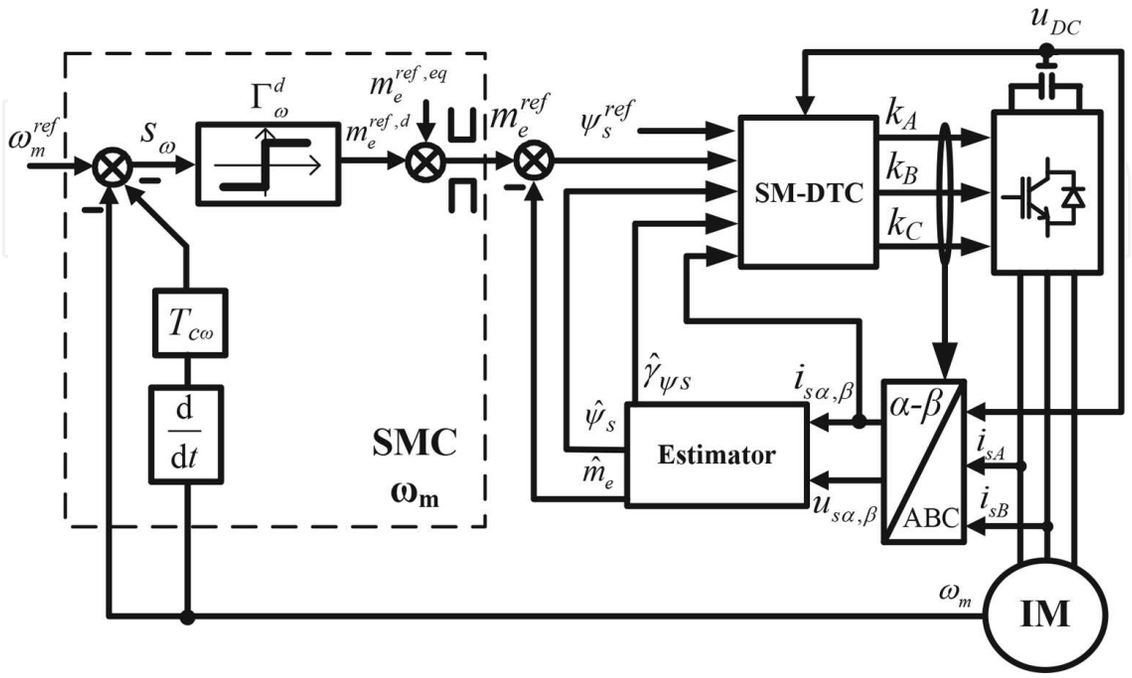

Figure 6. Block diagram of the SM speed control in cascade connection.

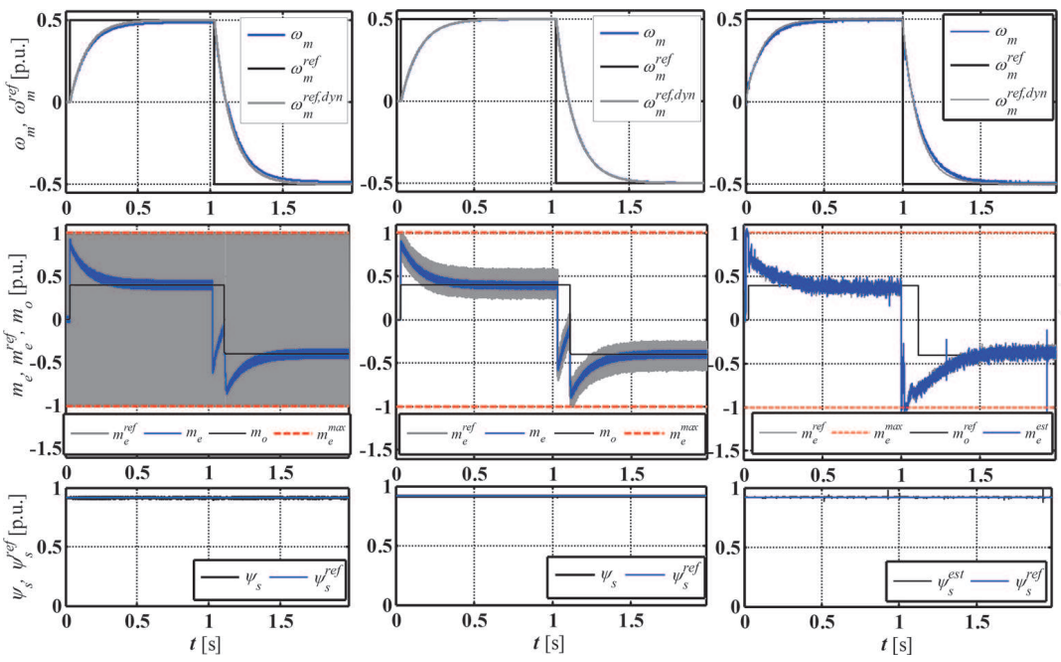

Figure 7. Performance of the SM cascade speed control: (a) simulation study: relay control, (b) simulation study: equivalent control, (c) experimental study: equivalent signal-based control; first row: reference and real speed, second row: load, electromagnetic and maximum torques, third row: reference and real amplitude of stator flux.

5. Sliding mode position control

5.1. Direct sliding mode position control

By the analogy to the torque and speed control, presented in previous sections, IM shaft position control can be designed using the direct approach [1]. The control algorithm [Eq. (12)] and the $\mathbf{D}_1$ matrix [Eq. (24)] remain the same as for the direct speed control, $T_{c\omega}$ is only replaced by $T_{c\theta}$. Switching function for the position control becomes:

$$s_1 = s_\theta = \alpha_1\left(\theta_m^{ref} - \theta_m - T_\theta\dot{\theta}_m - T_{c\theta}\ddot{\theta}_m\right) \tag{35}$$

where T_θ, $T_{c\theta}$ are time constants that can be selected according to the required settling time (5%) of the position control $T_{s\theta}$, using the following rule [27]:

$$T_\theta = 2T_{cr},\ T_{c\theta} = T_{cr}^2,\ T_{cr} = \frac{2T_{s\theta}}{9}. \tag{36}$$

The block diagram of the SM direct position control is presented in **Figure 8**. Performance of the SM direct position control during experimental tests is shown in **Figure 9**. It can be seen that the shaft position has the desired dynamics and tracks the reference value without almost any error. Unfortunately, the chattering visible in the torque is entirely unacceptable. Therefore, the saturation function is applied (**Figure 9b**)—the level of the undesired oscillations is greatly reduced. In both cases, similarly to the direct speed control, the electromagnetic torque is not supervised in this type of the control. Simultaneously, the speed does not exceed the accepted value, which is 120% of the nominal value in this research. The flux is kept constant (not shown in the figure).

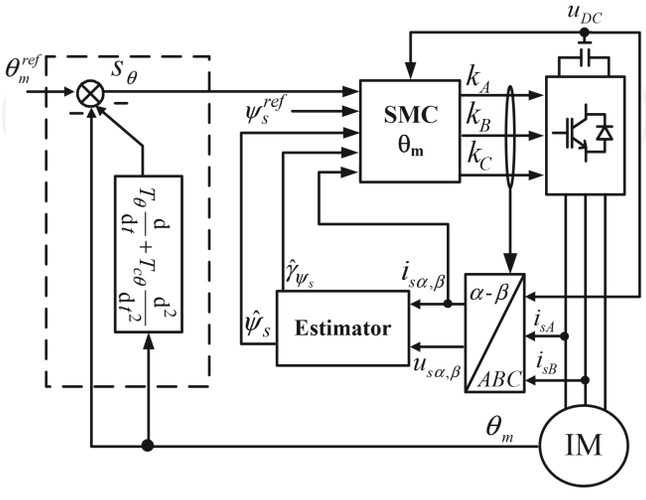

Figure 8. Block diagram of the direct SM position control.

http://dx.doi.org/10.5772/63407

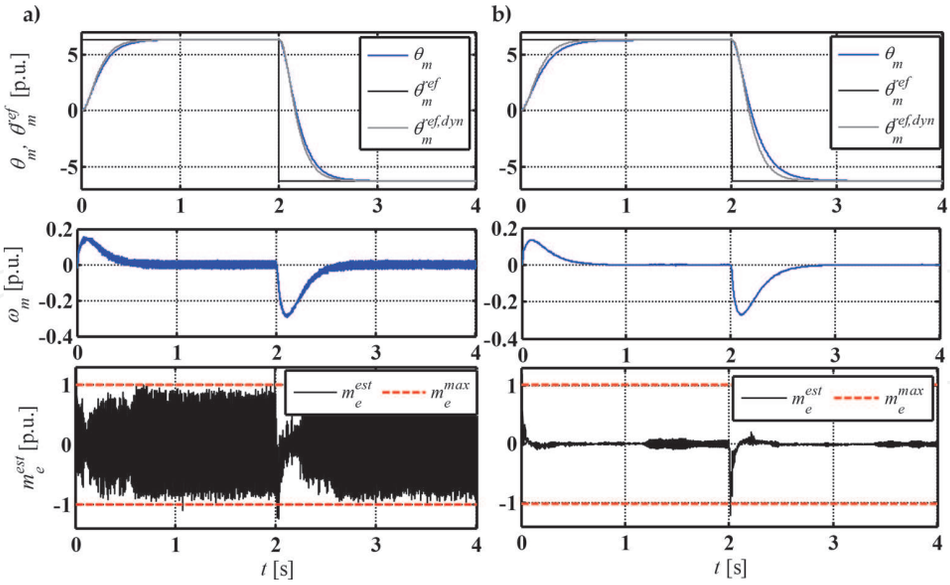

Figure 9. Experimental performance of the SM direct position control: (a) with sign function, (b) with saturation function.

5.2. Cascade sliding mode position control

According to the previous section, the cascade position control structure will now be analyzed. It is based on the assumption that the SM speed control works perfectly and ensures zero value of the speed switching function from Eq. (22). In such situation, the speed control loop can be described by the following transfer function:

$$\frac{\omega_m(p)}{\omega_m^{ref}(p)} = \frac{1}{T_{c\omega}p+1} \tag{37}$$

Similarly, as for the speed control, the control signals vector and switching functions' vector become scalars, $\mathbf{k}=[\omega_m^{ref}]$, $\mathbf{s}=[s_\theta]$, respectively. In this case, the switching function derivative becomes:

$$\dot{s}_\theta = f_{1\theta} + f_{2\theta} + d_\theta \omega_m^{ref}, \tag{38}$$

$$f_{1\theta} = \dot{\theta}_m^{ref} - \frac{1}{T_N}\left(\omega_m - \frac{T_\theta}{T_\omega}\right) - \frac{T_{c\omega}}{T_M T_N}\dot{m}_e, \tag{39}$$

$$f_{2\theta} = \frac{T_{c\theta}}{T_M T_N}\dot{m}_o, \tag{40}$$

$$d_\theta = -\frac{T_\theta}{T_N T_{c\omega}}. \tag{41}$$

By analogy to equation (30), the reference speed control signal is as follows:

$$\omega_m^{ref} = \omega_m^{ref,eq} + \omega_m^{ref,d}, \tag{42}$$

$$\omega_m^{ref,eq} = -\frac{1}{d_\theta} f_{1\theta}, \tag{43}$$

$$\omega_m^{ref,d} = -\frac{\Gamma_\theta^d}{d_\theta} \mathrm{sign}(s_\theta), \tag{44}$$

where Γ_θ^d is a control parameter.

According to the methodology shown in previous sections, the position control system is stable if:

$$\Gamma_\theta^d > |f_{2\theta}|. \tag{45}$$

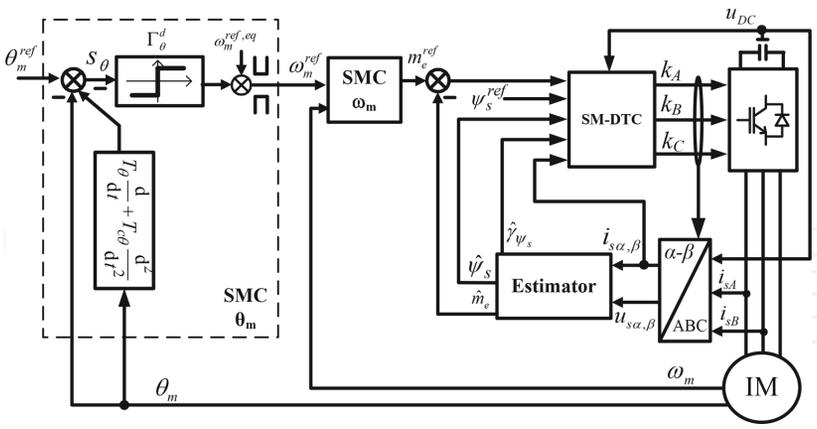

Figure 10. Block diagram of the cascade SM position control.

The block diagram of the proposed cascade position control structure is shown in the **Figure 10**. Performance of the control structure for nominal load operation is shown in **Figure 11**. First, the simulation study for the ideal case is shown (**Figure 11a**), the sign function is used in the control algorithm directly. It can be seen that the position follows the reference signal with required dynamics. Due to the torque constraint introduced, some small dynamical

http://dx.doi.org/10.5772/63407

error of the position control is visible. In order to decrease the level of the chattering of torque and speed, visible especially when the digital operation is taken into account (**Figure 11b**), the saturation function is applied in **Figure 11c**. The oscillations level is reduced successfully, while the position dynamic error is maintained. **Figure 11d** shows the experimental results—because of the digital realization of the control structure and additional, parasitic dynamics (measurement delays), the controlled variables are characterized by larger chattering; however, its level is acceptable. The position dynamic error is slightly higher than in case of the simulation tests.

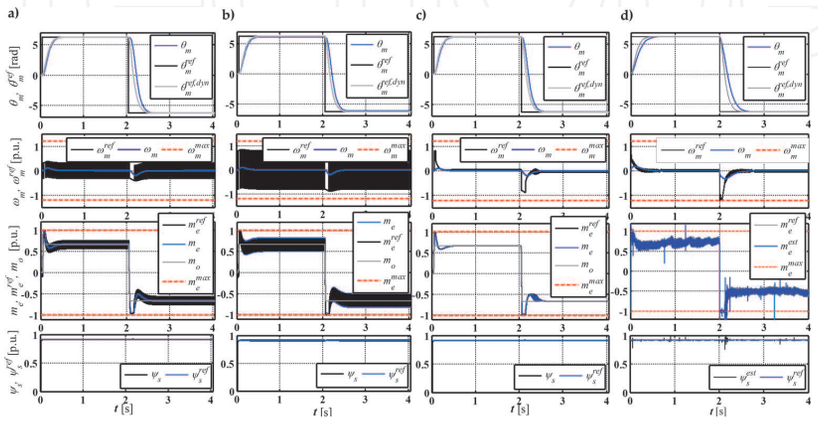

Figure 11. Performance of the SM equivalent control signal-based position control in a cascade structure: (a) simulation study: ideal case, (b) simulation study: digital operation and delays taken into account, (c) simulation study: saturation function used instead of the sign function in cascade control, (d) experimental results with saturation function used in cascade control; first row: reference and real position, second row: reference, real and maximum speed; third row: reference, real (estimated), load and maximum torque; fourth row: reference and real (estimated) stator flux amplitude.

6. Conclusions

This chapter deals with the SMC of the most important IM variables: torque, speed and position of the shaft, simultaneously ensuring constant value of the stator flux amplitude.

First part of the chapter is connected with the sliding mode DTC for IM. It is proved that the classical DT-SMC approach gives undesirable torque chattering. In order to reduce the chattering, the saturation function is used instead of the sign function. However, the saturation function introduces large steady-state control error. An integral part in the torque switching function is successfully used to eliminate this error. Such designed torque control is then used in the cascade speed and position IM control.

Next part of the chapter is the IM speed control. It is shown that the sliding mode speed control in its classical, direct approach is characterized by a large steady-state error and chattering. It is proved using a specially prepared simulation model and experimental setup. Additionally, the torque value is not constrained in this direct speed control structure. Therefore, the cascade connection of speed and torque regulators is introduced. The equivalent signal-based control method is applied to reduce the chattering. This solution allows to supervise the value of the electromagnetic torque, while reducing the control error effectively.

The last part of the chapter shows the position control of the drive. Conclusions that come from the SM position control analysis are analogical to the ones from the speed control. Direct position control does not ensure the torque and speed supervision, that is solved by the cascade control structure. Simultaneously, the chattering can be reduced using the continuous approximation of the sign function and the equivalent signal-based approach.

All of these control concepts are illustrated using simulation and experimental study. Special attention has been paid to create a simulation model that allows to take the digital realization of modern DSP control applications and measurement delays into account.

Acknowledgements

This work has been financed by the National Science Centre (Poland) under project number 2015/17/B/ST7/03846.

Appendices

Experimental tests were realized using the DSP dSpace 1103 with sampling time equal to 100 μs (10 kHz). The DSP controlled the transistors of the classical two-level VSI, which supplied the 3 kW tested motor. 6 kW DC motor was used to generate the load torque.

Tables 1–3 include rated values of the tested IM, its parameters and base values, necessary to make the transition from physical units to the p.u. system, respectively.

Name	Symbol	SI units		Normalized units [p.u.]
Voltage	U_N	400Δ/680Y	[V]	0.707
Current	N_N	7.0Δ/4.0Y	[A]	0.707
Power	P_N	3000	[W]	0.62
Torque	M_N	20.46	[Nm]	0.67
Rotational frequency	n_N	1400	[rpm]	0.933
Frequency	f_{SN}	50	[Hz]	1
Stator flux	Ψ_{sN}	1.65	[Wb]	0.91
Rotor flux	Ψ_{rN}	1.55	[Wb]	0.86
Pole pairs	p_b	2	[-]	2
Power factor	$\cos\varphi$	0.80	[-]	0.80
Efficiency	η	0.778	[-]	0.778

Table 1. Rated parameters of the tested induction motor.

http://dx.doi.org/10.5772/63407

Name	Symbol	SI units ([])		Normalized units [p.u.]
Stator resistance	R_s, r_s	7.073	[Ω]	0.707
Rotor resistance	R_r, r_r	7.372	[Ω]	0.737
Main inductance	L_m, l_m	597.8	[mH]	1.87
Stator leakage inductance	$L_{r\sigma}$, $l_{s\sigma}$	31.2	[mH]	0.098
Rotor leakage inductance	$L_{r\sigma}$, $l_{r\sigma}$	21.2	[mH]	0.066

Table 2. Equivalent circuit parameters of the tested induction motor.

Name	Expression	Value	Units
Power	$S_b = 3/2U_bI_b$	4800	[VA]
Torque	$M_b = p_bS_b/\Omega_b$	30.55	[Nm]
Speed	$N_b = 60f_{sN}/p_b$	1500	[rpm]
Stator voltage	$U_{sb} = \sqrt{2}U_{sN}$	565.7	[V]
Stator current	$I_{sb} = \sqrt{2}I_{sN}$	5.657	[A]
Frequency	$f_{sb} = f_{sN}$	50	[Hz]
Angular velocity	$\Omega_b = 2\pi f_{sN}$	100π	[rad/s]
Flux	$\Psi_b = U_b/\Omega_b$	1.80	[Wb]
Inductance	$L_b = \Psi_b/I_b$	0.318	[H]
Impedance	$Z_b = U_b/I_b$	100	[Ω]

Table 3. Calculation of per unit system base values.

Author details

Grzegorz Tarchała and Teresa Orłowska-Kowalska

*Address all correspondence to: grzegorz.tarchala@pwr.edu.pl

Department of Electrical Machines, Drives and Measurements, Wrocław University of Technology, Wrocław, Poland

References

[1] Utkin VI. Sliding mode control design principles and applications to electric drives. IEEE Trans Ind Electron. 1993;40(1):23-36.

[2] Shyu KK, Shieh HJ. A new switching surface sliding-mode speed control for induction motor drive systems. IEEE Trans Power Electron. 1996;11(4):660-7.

[3] Orłowska-Kowalska T, Tarchała G. Integral sliding mode direct torque control of the induction motor drives. 39th Annual Conference of the IEEE Industrial Electronics Society (IECON), November 10-13, 2013, Vienna, 2013, p. 8482-7.

[4] Dunnigan MW, Wade S, Williams BW, Yu X. Position control of a vector controlled induction machine using Slotine's sliding mode control approach. IEE Proc-Electr Power Appl. 1998;145(3):231-8.

[5] Wang WJ, Chen JY. A new sliding mode position controller with adaptive load torque estimator for an induction motor. IEEE Trans Energy Convers. 1999;14(3):413-8.

[6] Zhang Z, Zhu J, Tang R, Bai B, Zhang H. Second order sliding mode control of flux and torque for induction motor. Asia-Pacific Power and Energy Engineering Conference (APPEEC), March 28-31, 2010, Chengdu, 2010, p. 1-4.

[7] Rashed M, Goh KB, Dunnigan MW, MacConnell P, Stronach A, Williams BW. Sensorless second-order sliding-mode speed control of a voltage-fed induction-motor drive using nonlinear state feedback. IEE Proc-Electr Power Appl. 2005;152(5):1127-36.

[8] Bartolini G, Marchesoni M, Pisu P, Usai E. Chattering reduction and robust position control in induction motor with second-order VSS. Int J Syst Sci. 1998;29(1):1-12.

[9] Ferrara A, Rubagotti M. A sub-optimal second order sliding mode controller for current-fed induction motors. American Control Conference, June 10-12; St Louis, MO: IEEE; 2009, p. 59-64.

[10] Comanescu M, Batzel T. A novel speed estimator for induction motor based on integral sliding mode current control. IEEE Power & Energy Society General Meeting, 2008, p. 371-6.

[11] Comanescu M, Xu L, Batzel TD. Decoupled current control of sensorless induction-motor drives by integral sliding mode. IEEE Trans Ind Electron. 2008;55(11):3836-45.

[12] Comanescu M. An induction-motor speed estimator based on integral sliding-mode current control. IEEE Trans Ind Electron. 2009;56(9):3414-23.

[13] Veselic B, Perunicic-Drazenovic B, Milosavljevic C. High-performance position control of induction motor using discrete-time sliding-mode control. IEEE Trans Ind Electron. 2008;55(11):3809-17.

[14] Veselic B, Perunicic-Drazenovic B, Milosavljevic C. Improved discrete-time sliding-mode position control using euler velocity estimation. IEEE Trans Ind Electron. 2010;57(11):3840-7.

[15] Castillo-Toledo B, Di Gennaro S, Loukianov AG, Rivera J. Discrete time sliding mode control with application to induction motors. Automatica. 2008;44(12):3036-45.

[16] Lascu C, Boldea I, Blaabjerg F. Variable-structure direct torque control: A class of fast and robust controllers for induction machine drives. IEEE Trans Ind Electron. 2004;51(4):785-92.

[17] Lascu C, Trzynadlowski AM. Combining the principles of sliding mode, direct torque control, and space-vector modulation in a high-performance sensorless AC drive. IEEE Trans Ind Appl. 2004;40(1):170-7.

[18] Derdiyok A, Guven MK, Inanc N, Rehman H, Xu LY. A DSP-based indirect field oriented induction machine control by using chattering-free sliding mode. IEEE National Aerospace and Electronics Conference: Engineering Tomorrow. Dayton, Ohio, USA 2000:568-73.

[19] Wai RJ. Adaptive sliding-mode control for induction servomotor drive. IEE Proc-Electr Power Appl. 2000;147(6):553-62.

[20] Betin F, Capolino G-A. Sliding mode control for an induction machine submitted to large variations of mechanical configuration. Int J Adapt Control Signal Process. 2007;21(8-9):745-63.

[21] Tarchała G, Orłowska-Kowalska T. Application of a time-varying switching line in the cascade sliding-mode speed control of the induction motor drive. IEEE 23rd International Symposium on Industrial Electronics (ISIE), June 1-4, 2014, Istanbul, 2014, p. 1310-5.

[22] Kaźmierkowski MP, Tunia H. Automatic Control of Converter-Fed Drives. Elsevier Science; 1994.

[23] Holtz J, Quan JT. Drift- and parameter-compensated flux estimator for persistent zero-stator-frequency operation of sensorless-controlled induction motors. IEEE Trans Ind Appl. 2003;39(4):1052-60.

[24] Levant A. Chattering analysis. IEEE Trans Automat Control. 2010;55(6):1380-9.

[25] Utkin V, Lee H. Chattering problem in sliding mode control systems. International Workshop on Variable Structure Systems. Alghero, Sardinia, Italy 2006:346-50.

[26] Orłowska-Kowalska T, Tarchała G. Unified approach to the sliding-mode control and state estimation - application to the induction motor drive. Bull Pol Acad Sci-Tech Sci. 2013;61(4):837-46.

[27] Dodds SJ. Settling time formulae for the design of control systems with linear closed loop dynamics. 3rd Annual Conference Advances in Computing and Technology: The School of Computing and Technology, University of East London, UK; 2008, p. 31-9.

IntechOpen